Microfluid Nanofluid (2012) 13:543–554
DOI 10.1007/s10404-012-0995-6

RESEARCH PAPER

On the direct employment of dipolar particle interaction in microfluidic systems

Frank Wittbracht · Alexander Weddemann · Bernhard Eickenberg · Andreas Hütten

Received: 7 February 2012 / Accepted: 1 May 2012 / Published online: 19 May 2012

Abstract This review article will summarize recent developments in the employment of dipolar coupled magnetic particle structures. We will discuss the basics of magnetic dipolar particle interaction in static and rotating magnetic fields. In dependence on the magnetic fields employed, agglomerates of different dimensionality may form within the carrier liquid. The stability and formation dynamics of these particle structures will be presented. Furthermore, we will review recent microfluidic applications based on the interaction of magnetic particles and present methods for surface patterning with micron-sized and nano-sized particles which employ dipolar particle coupling.

1 Introduction

Many research groups have employed magnetic particles and beads in microfluidic systems, and such colloids have been established as a vital component in MEMS and NEMS devices (Gijs 2004, Pamme 2006; Niarchos 2003; Deng et al. 2001; Zhu et al. 2010). A key role is played by superparamagnetic microbeads which consist of superparamagnetic nanoparticles embedded in a polymer matrix (Haukanes and Kvam 1993). Due to their magnetic content, particles may be manipulated by either on-chip or off-chip generated magnetic fields. An external field generation may significantly reduce the complexity of the device, since many additional microstructured components become obsolete. On the other hand, the magnetic colloids themselves introduce a magnetic gradient on the microscale. These field contributions and the entailed magnetic interplay may strongly influence the fluid velocity as it can be seen in the example of ferrofluids or magnetorheological liquids (Shliomis and Morozov 1994; Love et al. 2005; Rosensweig 1996; Zahn and Pioch 1999; Moskowitz and Rosensweig 1967; Ginder et al. 1996; Ginder and Davis 1994; Mao et al. 2011; Kose et al. 2009). In fact, this is only the case if a high concentration of magnetic particles is present within the suspension. Many applications operate in the low concentration limit and particle–particle couplings can be omitted (Pamme and Manz 2003; Weddemann et al. 2009; Østergaard et al. 1999). The region in between these extreme scenarios has only recently attracted attention. The cases described above can be modeled in the frame of continuum theories (Tang and Conrad 2000; Yeh and Chen 1997; Brigadnov and Dorfmann 2005; Zhu et al. 2011a, b). In contrast, the intermediate state combines properties of the continuum fluid flow with discrete particle dynamics (Laroze et al. 2008; Mørup et al. 2010; Kim and Park 2010).

However, such an approach offers new possibilities to assign different functional tasks to the particle suspension, which can be activated if an external magnetic field is switched on. In a similar way, Erickson et al. have developed on-demand configurable matter (Kalontarov et al. 2009) suspended in a carrier liquid, based on anisotropic porosity for hydrodynamically driven self-assembly. A similar approach would be helpful for magneto-based microfluidics. Sawetzki et al. (2008) presented the employment of clusters

F. Wittbracht (✉) · B. Eickenberg · A. Hütten
Department of Physics, Thin Films and Physics of Nanostructures, Bielefeld University, PB 100131, 33501 Bielefeld, Germany
e-mail: fwittbra@physik.uni-bielefeld.de

A. Weddemann
Department of Electrical Engineering and Computer Science, Research Laboratory of Electronics/Laboratory for Electromagnetic and Electronic Systems, Massachusetts Institute of Technology, 77 Massachusetts Avenue, Cambridge, MA 02139, USA

of paramagnetic particles for mixing and flow guiding design. However, the cluster preparation is achieved by optical tweezers and, thus, not transferable to lab-on-a-chip systems.

In order to establish such intermediate concentration states as a valuable tool for new microfluidic devices and allow for the direct employment of their magnetic coupling as additional degrees of freedom, we will summarize recent advances on their fundamental properties and cluster formation dynamics. We will review important step-stones and first devices which already employ these techniques. Finally, we will discuss the possibility of transferring such mechanisms to even lower size scales.

2 Magnetic dipole interaction

For microfluidic applications, superparamagnetic particles are mainly used. Their magnetic moment can be adjusted by external field contributions and they demagnetize on short timescales once the perturbation is switched off again. At room temperature, the magnetic state of free particles is governed by thermal contributions which exceed the inner anisotropy energy. Such interplay results in a rapidly fluctuating orientation direction of the magnetic moment, where orientation changes occur on smaller timescales than the minimum measurements scales. Consequently, a free particle resembles a non-magnetic characteristic. If the particle is brought into a magnetic field, a resulting torque leads to the alignment of moment vector and field axis, which reduces the fluctuation and entails an effective magnetic moment $\boldsymbol{m}$. Small particles are usually homogeneously magnetized and, hence, the external magnetic field $\boldsymbol{H}$ is given by the dipolar expression (Jackson 1975)

$$H(r) = \frac{1}{4\pi}\left(\frac{3\langle m\,,\, r\rangle\, r}{r^5} - \frac{m}{r^3}\right) \tag{1}$$

where $\langle \bullet\,,\, \bullet\rangle$denotes the Euclidian inner product.

The force which acts on a particle with magnetic moment $\boldsymbol{m}$ exposed to an external magnetic field $\boldsymbol{H}_{\text{ext}}$ is given by (Zborowski et al. 1999)

$$F_{\text{part}} = \mu_0 \left(m_{\text{part}} \cdot \nabla\right) H_{\text{ext}} \tag{2}$$

with μ_0 the permeability of the vacuum. In particular, no resulting forces can be reported if magnetic objects are placed in a homogeneous magnetic field. However, a particle feels the inhomogeneous field contribution of magnetic colloids nearby. Therefore, for sufficiently high particle concentrations, the interparticular exchange becomes increasingly important. Such interactions may result in agglomeration of contiguous magnetic objects as schematically summarized in Fig. 1. If the distance between two particles is not too high, the alignment of their magnetic moment vectors entails an attractive force which leads to the formation of one-dimensional chain structures. (Fig. 1a–c). The chain direction is parallel to the field axis as long as viscous drag forces are small enough to be omitted. The chain orientation follows the field vector if changes are carried out adiabatically. The chain rotation is damped by the viscosity of the carrier liquid, which exerts shear forces along the chain and leads to a phase lag resulting in a mismatch of the chain direction and magnetic field orientation. If the angular field velocities exceed a critical limit, stresses surpass the breaking point of the chain and such rod structures cannot maintain their stability. As we will see later on, chain breakage is followed by reorganization of particles in two-dimensional sheets. The inner magnetic distribution strongly governs their properties (Weddemann et al. 2010a).

The dimensionless Mason number gives a first estimation of the governing physical driving force by comparison of typical scales of hydrodynamic and magnetic contributions. Different definitions of the Mason number can be found in the literature (Melle et al. 2003; Bossis et al. 2002). We will focus on the definition given by Petousis et al. (2007):

$$Mn = \frac{16\eta\omega}{\mu_0 \chi^2 H^2} \tag{3}$$

where η is the viscosity of the fluid surrounding the particles, ω the angular velocity of the magnetic field, χ the effective dimensionless susceptibility of the beads and H denotes the field strength. The Mason number was originally introduced in a different form for the study of electrorheological fluids under shear stress (Gast and Zukoski 1989).

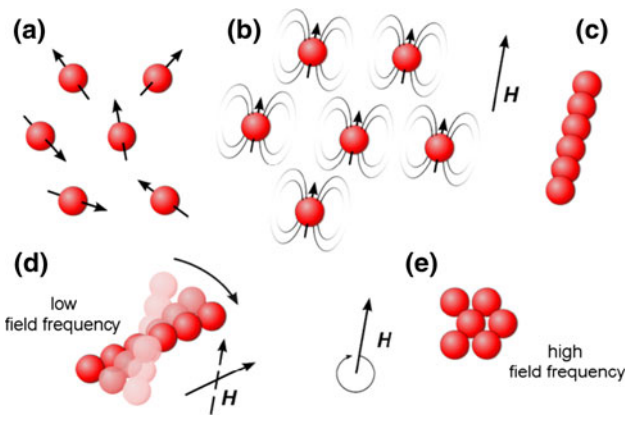

Fig. 1 Schematic representation of the magnetic field-induced assembly of magnetic particles for different configurations of the external magnetic field

3 Stability and formation dynamics of dipolar superstructures

A first step in the development of functional components assembled by magnetic particles is to understand their fundamental properties and the governing dynamics during the interaction. For the understanding of the magnetic force contributions, it is sufficient to discuss microscaled systems which ease the analysis due to the possibility to dynamically observe all processes by optical microscopy. All experiments and results presented in this chapter are based on micron-sized magnetic beads. A first transition to the nanoscale will be presented in Sect. 5.2.

3.1 One-dimensional agglomerates

Numerous research groups investigated the fundamental behavior and stability of one-dimensional agglomerates. The properties of such combined objects were analyzed in dependency on the external field characteristics. From Eqs. (1) and (2), we immediately learn that the forces between two adjacent particles increase with the magnetic moments involved. Consequently, a high magnetization entails strong chain stability. Furst and Gast were able to directly prove this relation. They analyzed the micromechanics of dipolar particle chains by force spectroscopy (Furst and Gast 1999). Dual-trap optical tweezers were employed to determine rupture forces of the particle chains parallel and perpendicular to the applied magnetic field direction. Experiments were performed with 0.85-μm polystyrene particles with embedded monodomain iron-oxide particles. These micron-sized colloids form superparamagnetic beads. Typical rupture forces of particle chains as determined by Furst and Gast lie in the range of 6.4 to 45 pN depending on the dipole strength.

The influence of a rotating magnetic field on paramagnetic particle chains was investigated by Vuppu et al. (2003) by video microscopy of rotating chains immersed in a carrier liquid. Up to a critical rotation frequency, the angular velocity of chain and field rotation was identical. A further increase of the frequency resulted in breakage and reordering due to the viscous drag forces parallel to the chain axis. In particular, they were able to show the existence of an S-shaped dislocation of individual particles in the assembly in the frequency transition regime. At such frequencies, magnetic cohesion and viscous shear are on the same size scale. Such S-dislocated states were further investigated by Petousis et al. (2007), who characterized the chain breaking event in dependence on the Mason number and length of individual chains. Within their works, they developed a discrete theoretical model which resulted in the finding that the maximum number of particles in a stable chain is proportional to $Mn^{-1/2}$.

The regime of frequencies past the breaking has only been characterized recently (Wittbracht et al. 2011). In addition to a decreasing mean chain length with increasing rotation frequency of the applied magnetic field, the formation of two-dimensional agglomerates can be observed. For a quantitative analysis of the transient dynamics, particle structures were divided into three different classes: (1) bead clusters, (2) bead chains and (3) isolated particles. Such classification is visualized in Fig. 2. Analyses of the harmonic equilibrium states were carried out for three different particle concentrations of 83, 100 and 125 μg/ml. The chain length at a certain frequency decreases with increasing particle concentration. The reduction of chain lengths can be related to the growth dynamics of two-dimensional superstructures. Cluster formation comes at the cost of chain length. This result can be qualitatively understood similar to the LaMer model in the case of nanoparticle fabrication (LaMer and Dinegar 1950). Initial nuclei are only formed where the local concentration exceeds a critical threshold. These nuclei attract particles within the surrounding area and, consequently, the more of them are formed, the fewer particles remain in chain structures. Also, with more clusters in the sample, chains have a higher probability to be absorbed by two-dimensional structures. This probability is increased with the area a chain travels and, therefore, higher for longer chains.

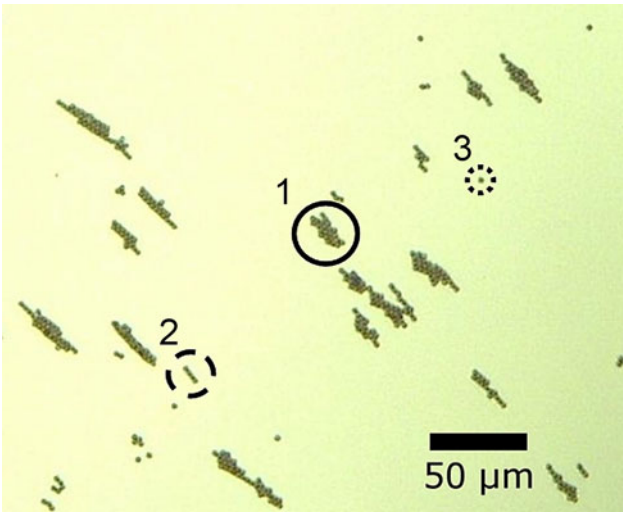

Fig. 2 Optical microscopy image of Dynabeads M-280 under the influence of a rotating magnetic field. Structures are classified according to their dimension (reprinted with permission from Wittbracht et al. 2011. Copyright 2011, American Institute of Physics)

3.2 Two-dimensional agglomerates

Other aspects of dynamics become visible if the object ratios of object classes 1–3 are considered. These ratios are defined by

$$\chi_{\text{bead}}^{\text{obj}} = \frac{N_{\text{obj}}(t)}{N_{\text{all}}(t)} \tag{4}$$

where N_{obj} and N_{all} denote the time-dependent number of magnetic particles in a certain object class and the overall number of particles within the sample, respectively. The resulting time dependence of $\chi_{\text{bead}}^{\text{obj}}$ for different objects and rotation frequencies is summarized in Fig. 3.

As seen in Fig. 3a, cluster formation occurs during the first few 10 s of magnetic field exposure. During this time period, a reordering process from one-dimensional to two-dimensional structures is found, which manifests itself in the strong reduction of the chain concentration (Fig. 3b). The bead ratio of free particles shows no significant time dependence. The small variations of the bead ratio for free particles as time evolves can be attributed to statistical fluctuations and can consequently be omitted for the growth dynamics of clusters. Cluster formation, which is governed by the addition of chains, can be compared to the deposition of monomers during growth of nanoparticles (Sugimoto 2001). Hence, a similar modeling approach for the evaluation of the concentration evolution should be possible. The decay of concentration of chain structures $\chi_{\text{bead}}^{\text{chain}}$ is assumed to be proportional to the concentration itself and, consequently, the cluster growth follows the exponential law with a rotation frequency-dependent chain dissociation rate a_{chain}.

$$\chi_{\text{bead}}^{\text{cluster}}(t) = 1 - \exp(-a_{\text{chain}}(f)t) \tag{5}$$

In general, the chain dissociation rate would be expected to be dependent on the Mason number, but as only the rotation frequency of the magnetic field is changed in the experiments, we will limit the analysis to the frequency dependence of a_{chain}, which can be obtained from the data presented in Fig. 3b if the data points are fitted according to Eq. (5). Numeric results are shown in Fig. 3c and a linear frequency dependence of the chain dissociation rate is found for the analyzed rotation states. These results do not contradict the findings of Petousis et al. (2007), since the proportionality to $Mn^{-1/2}$ and in particular to $f^{-1/2}$ was reported for a wider frequency regime.

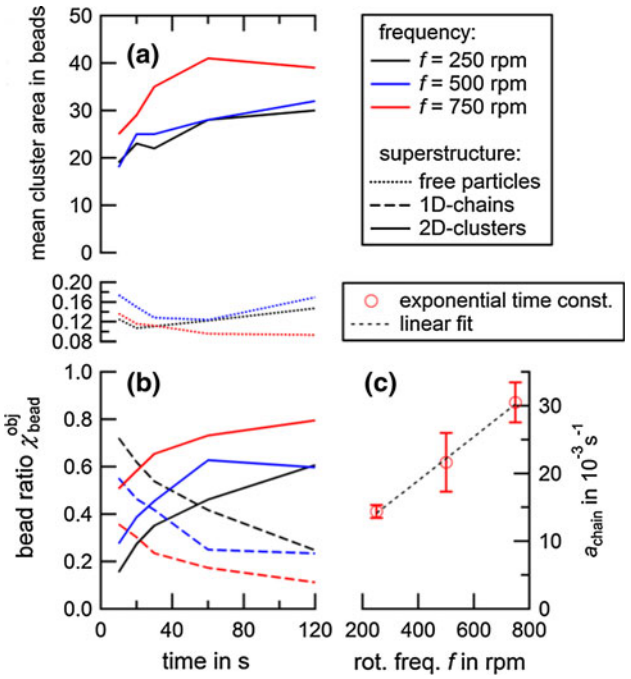

Fig. 3 Cluster growth dynamics. **a** Mean cluster areas increase while time evolves for all investigated rotation frequencies. **b** Evolution of the bead ratio for single particles (*dotted*), chains (*dashed*) and clusters (*solid*). **c** Frequency dependence of the time constant a_{chain} obtained from exponential fit of the data presented in subplot (**b**) (reprinted with permission from Wittbracht et al. 2011. Copyright 2011, American Institute of Physics)

4 Direct employment of dipolar coupling in microfluidic devices

The formation and stability properties of assemblies of magnetic beads form the fundamental basis for their employment as functional components in microfluidic devices. Depending on their dimension which results from the magnetic field employed as described above, various applications are possible.

4.1 Static magnetic field applications

Dipolar interaction of magnetic particles at particle concentrations sufficient for the formation of one-dimensional superstructures was used by Lacharme et al. (2009) to realize an on-chip immunoassay based on the retention of superstructures within a microfluidic channel as presented in Fig. 4. For the experiments, a straight channel with grooves along the channel walls was employed. Particle superstructures (bright lines) are trapped at defined channel positions if a static magnetic field perpendicular to the flow direction is applied. As described above, these chains are stable up to a critical flow velocity value which limits the throughput of the procedure. The superstructures were estimated to be approximately 1.5-μm wide and consist of 500-nm particles. If a classification as above is applied, these structures may be categorized as chain-like agglomerates.

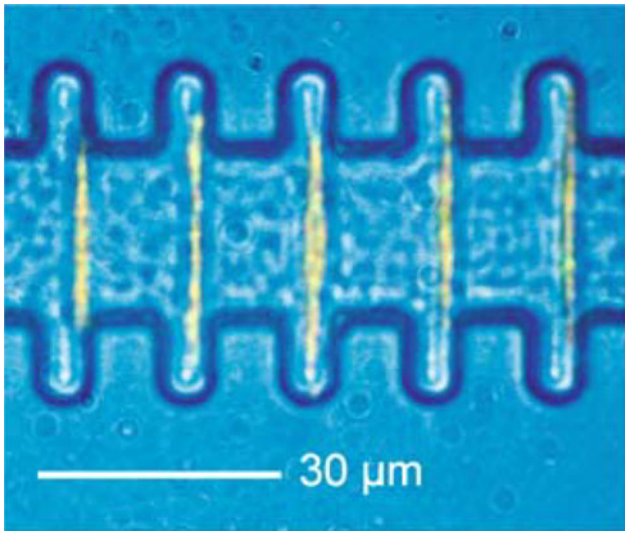

Fig. 4 Optical microscopy image of magnetic particle chains within the retention junction of the microfluidic structure proposed by Lacharme et al. for on-chip sandwich immunoassays (with kind permission from Springer Science + Business Media: Lacharme et al. (2009), Fig. 4a)

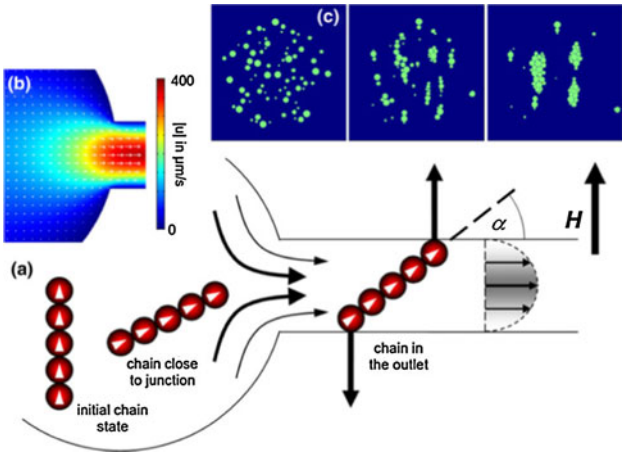

Fig. 5 **a** Schematic illustration of the operation principle of the investigated microfluidic device for particle flow control. **b** Calculated hydrodynamic velocity field at the reservoir channel junction. **c** Chain creation results from the dipolar coupling of magnetic particles in a static external magnetic field (with kind permission from Springer Science + Business Media: Weddemann et al. (2011), Fig. 1)

Based on this method, Lacharme et al. (2009) were able to detect mouse monoclonal target antibodies in both off-chip and on-chip incubation protocols. In particular, the on-chip protocol allows for the fluorescence-based detection of antibodies down to a concentration of a few ng/ml.

The design described above uncouples the particle velocity from the motion state of the carrier liquid by the employment of steric traps. This principle can be further developed to a dynamic guidance device if the stationary magnetic field is replaced by a rotating one. A first design based on free-flowing particle chains (Weddemann et al. 2011) which is operated by hydrostatic pressure is schematically shown in Fig. 5. The central component is formed by a circular reservoir connected to a straight channel. Perpendicular to the channel, parallel to the sample plane, a homogeneous magnetic field is applied. As before, a chain creation is entailed as schematically presented in Fig. 5c. The overall orientation of a chain is influenced by the superposition of the magnetic torque, which results from the interaction of the magnetic field and the magnetic moment vector, and induced hydrodynamic angular momentum density (Fig. 5a). The latter ones may gain significant importance within the junction area due to an asymmetric velocity profile (Fig. 5b). Therefore, even chains of lengths longer than the channel width can enter the channel. This process is reversible under the constraint of maintaining the chain structure by a rotation of the magnetic field in a direction parallel to the flow. In case of multiple reservoir exits of different orientations, the setting of the field direction acts as flow control for magnetic particles. A realization of this principle is shown in Fig. 6a; the particle flow to the reaction chamber R can be controlled by the direction of the external magnetic field. The particle flow from the inlet channels I_B and I_D to the reaction site can be initialized by the respective choice of the magnetic field orientation in the directions B and D. Similarly, the *drain* and *waste* channels can be addressed to collect the reaction product or residual solution, respectively. In Fig. 6b, the experimental realization of the PDMS channel structure is presented. The device can in principle be extended for additional inlet reservoirs (Fig. 6c). To demonstrate the operation principle, two different bead species of distinguishable sizes were employed. Respective solutions of 2.8-µm M-280 beads and 1.05-µm MyOne^{TM} were deposited in the inlet chambers I_D and I_B. The corresponding flow directions will be denoted by D and B in the following (compare Fig. 6a). A particle flow from one of the bead reservoirs to the reaction chamber R may be initiated or inhibited by a rotation of the magnetic field direction. Figure 7 shows an image sequence obtained by video microscopy of a typical fill/drain process. To ease the tracking of different bead species, M-280 beads are highlighted in red and MyOne^{TM} beads are colored in blue.

An initial field orientation D entails a particle flow of M-280 beads into the reaction chamber (Fig. 7a, b). This initial particle flow is blocked while beads from reservoir I_B begin to travel to the reaction site if the field direction is rotated parallel to the B axis (Fig. 7d, e). Subplots (d–f) show a chain of MyOne^{TM} beads which enters the reaction chamber and merges with a residual chain. Upon assembly, the large agglomerate can be washed down the drain if the magnetic field is aligned with direction C (Fig. 7f–i).

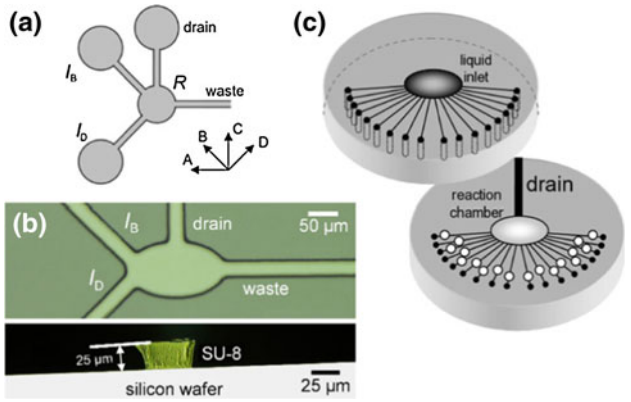

Fig. 6 **a** Schematic representation of the microfluidic channel geometry. **b** Optical microscopy image of the PDMS channel structure (*top*) and the SU-8 mold which indicates the channel dimensions (*bottom*). **c** A possible extension of the proposed device for multiple inlet channels (with kind permission from Springer Science + Business Media: Weddemann et al. (2011), Fig. 2)

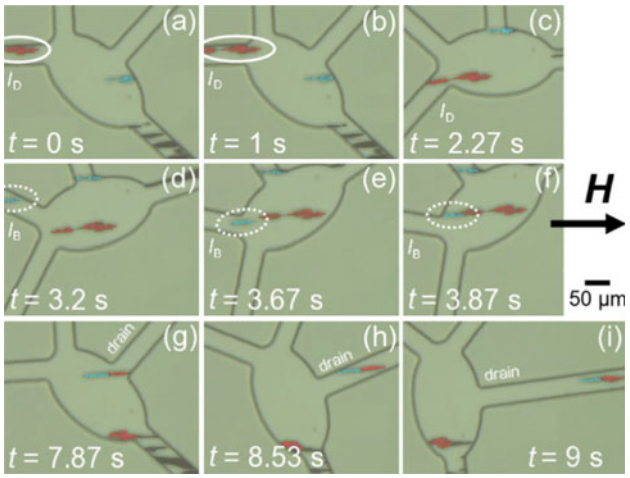

Fig. 7 Sequence of optical microscopy images during operation of the proposed microfluidic structure. The flow of particles from different reservoirs and inlet channels can be controlled by the field direction. In particular, the microfluidic channel design allows for the merging of chain segments of different bead species to confined objects. After a controlled combination, the product may afterward be washed out of the reaction chamber through the drain channel (with kind permission from Springer Science + Business Media: Weddemann et al. (2011), Fig. 3)

Fragmentation of bead chains within the reaction site can be observed due to the interaction of chain structure with the chamber walls while the field orientation is changed. Depending on the application, different optimizations need to be considered to avoid the breaking of superstructures. However, the proposed device proves the operation principle. Also, it shows that the idea of the direct employment of dipolar particle coupling for particle flow control for free-flowing components is valid and that the flow control is possible without the integration of electromagnetic components on the microscale.

The application described above demonstrates how the flow of the carrier liquid and the particle velocity may be uncoupled from each other. A different way to assign the direct interaction between magnetic particles to a functional task was introduced by Derks et al. (2010), who designed a micropump for fluidic devices. As explained by Eq. (2), a magnetic gradient field generates a magnetic force on magnetic material. If an object is pulled through a viscous liquid, an adjacent layer is dragged along, which results in a flow profile parallel to the object itself. To increase the impact of such particle motion, the authors applied two types of magnetic fields: a homogeneous field perpendicular to the flow direction for the generation of magnetic beads chains and a magnetic gradient field with a field derivative antiparallel to the fluid flow. Derks et al. (2010) demonstrated an experimental realization of this application and also introduced a numerical model, which predicts the pump efficiency of the proposed device based on the drag contributions of one-dimensional particle chains and isolated beads.

4.2 Microfluidic devices based on rotating magnetic fields

A refinement of the flow control device presented in Sect. 4.1 was recently proposed by Karle et al. (2011). Through the employment of a rotating magnetic gradient field, Karle et al. (2011) achieved the counterflow motion of two-dimensional agglomerates of dipolar coupled magnetic particles. The assembled particle structures have a length of about 200 µm and low aspect ratios between 3:1 and 5:1. The field gradient results in a magnetic force which drags the particle structures toward the channel wall. Under the influence of the field rotation, the agglomerates spin within the channel and periodically touch the channel walls. The friction between the channel geometry and the ends of the bead chains result in a linear momentum, which may push the chains against the flow direction $\boldsymbol{u}$ if $|u \times \tau| > 0$ with $\boldsymbol{\tau}$ the rotation axis of the magnetic field. The authors determined a maximum counterflow velocity of about 8 mm/s.

In addition, the interaction between two-dimensional particle superstructures and channel walls can be used as a mechanism for colloidal separation in microfluidic devices (Wittbracht et al. 2012). To demonstrate this technique, a channel geometry is chosen which includes a separation junction where a straight channel splits into two branches as shown in Fig. 8. The operation mode of the device is schematically illustrated in subplot (a). Magnetic particle superstructures are formed under the influence of a rotating magnetic field. These objects conduct stable rotations in the inlet channel. At the separation junction, the superstructures interact with the barrier between the daughter channels. In dependence of the rotation direction of the

colloidal agglomerates, particle structures may enter the daughter channels A or B. A quantitative analysis of the device results in separation efficiencies of up to 80 % if flow rates of up to 100 μm/s and rotation frequencies of 50 rpm are applied.

In addition to the separation of colloidal agglomerates from the carrier liquid stream, the channel design presented in Fig. 8 also allows for enhanced mixing by the employment of magnetically actuated free-flowing microstirrers. For a test demonstration, the inlet reservoirs I_1 and I_2 are filled with two different solutions, and magnetic beads are only suspended in inlet I_1. Similar to that in the linear motor presented by Derks et al. (2010), the chain rotation induces a convective flux nearby the chain position. Therefore, the fluid flow profile gains additional velocity components perpendicular to the flow direction, which entails an effective increased mixing of the two phases past the *T*-junction. Figure 9a images the alteration of flow. To easily distinguish between the two phases, the inlet I_2 is filled with a FAD solution which shows a dark contrast in microscopy images. Further, the interface was manually highlighted in red.

To quantitatively analyze the mixing efficiency, intensity profiles along the exit of the *T*-junction shown in Fig. 9a were evaluated. Figure 9b summarizes various intensity plots. We find a clear shift from the unperturbed boundary layer (black, solid) to the result obtained if rotating superstructures are present (red, solid). An effective diffusion constant may be calculated if the data obtained are compared to the analytic solution of a free diffusion across a boundary layer. In the case of sole thermal diffusion (Fig. 9b, black, dotted), a diffusivity of $D_0 = 3.04 \times 10^{-10}$ m^2/s is found which is in good agreement with the findings reported by Radoszkowicz et al. (2011). In the presence of magnetic microstirrers, the diffusion increases by 32 % in comparison to the thermal reference.

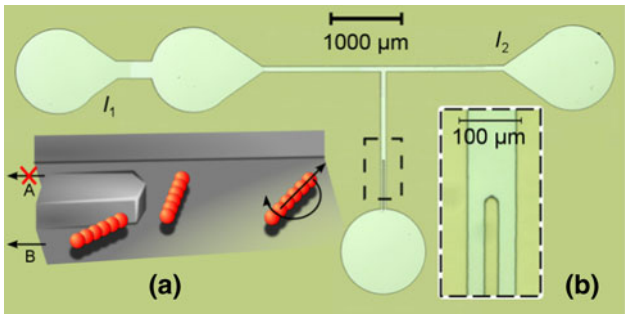

Fig. 8 Optical microscopy images of the microfluidic device for colloidal separation. **a** Particle agglomerates are guided into one of either channels based on the rotation direction. **b** The separation region consists of a straight channel, which splits up into two daughter channels (reprinted with permission from Wittbracht et al. 2012. Copyright 2012, American Institute of Physics)

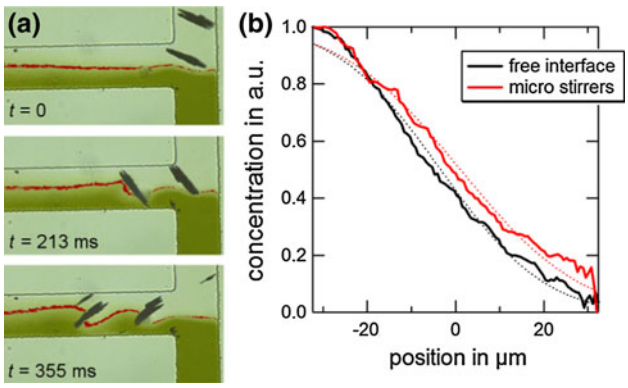

Fig. 9 **a** Rotation of the magnetic agglomerates at the interface layer between an FAD solution and water leads to a distortion of the boundary layer. **b** Intensity plots allow for an estimation of the resulting effective diffusion constants (reprinted with permission from Wittbracht et al. 2012. Copyright 2012, American Institute of Physics)

5 Surface patterning based on magnetically induced self-assembly of magnetic particles

5.1 Micron-sized particles in rotating magnetic fields

The assembly of particles in a rotating magnetic field in two-dimensional sheet-like structures at sufficiently high rotation frequencies of the external magnetic field may also be employed for the generation of large areas of highly ordered particle arrays. Two-dimensional clusters of superparamagnetic microparticles can be assembled and disassembled on-demand if the magnetic field is switched on or off, respectively. As was recently shown (Weddemann et al. 2010a), the exposure of magnetic microbeads to a homogeneous time-harmonic field results in highly ordered bead monolayers. The experiments presented here were carried out with magnetic beads with a mean diameter of 2.8 μm and a standard deviation of below 2 % (Fonnum et al. 2005). The suspension was placed on a silicon wafer in a spotting procedure and, afterward, immersed in a rotating field at a field strength of 390 Oe. The self-assembly of sheet-like structures inside the droplet was monitored by optical video microscopy. After evaporation of the carrier liquid, the resulting agglomerates were analyzed with respect to size and defect concentration. The influences of particle concentration and rotation frequency of the magnetic field were studied. Image sequences obtained from video microscopy of the particle solutions under the influence of the external magnetic field are shown in Fig. 10a–c. In Fig. 10a, cluster growth by adsorption of a one-dimensional particle chain to a previously formed cluster agglomerate is shown. During

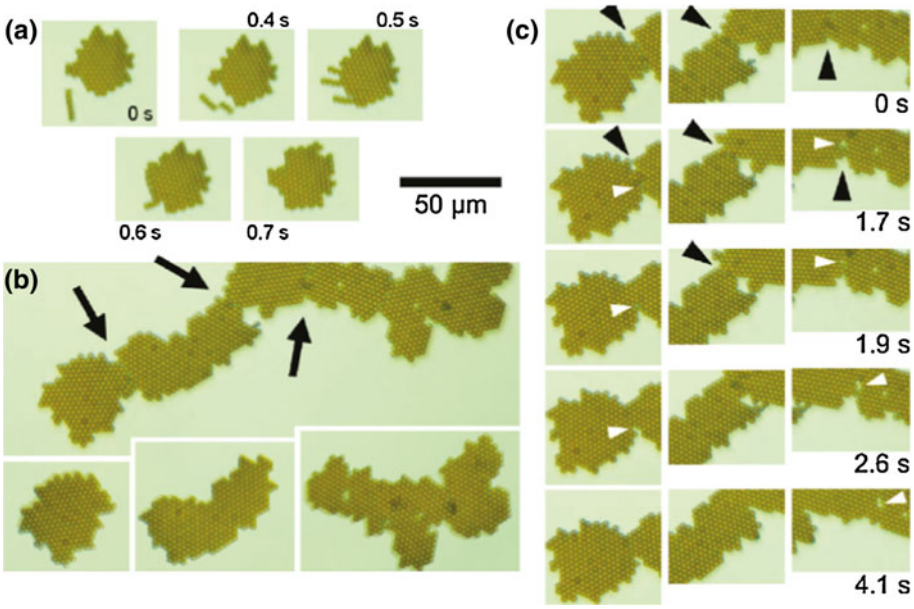

Fig. 10 Dynamic reordering processes under the influence of a rotating magnetic field. **a** A chain approaches a two-dimensional cluster object and adsorbs at the cluster surface. **b**, **c** Merging of clusters results in grain structures. Reorganization processes may lead to a homogeneous structure if enough free space is available (reprinted with permission from Weddemann et al. 2010a. Copyright 2010, American Chemical Society)

adsorption, the chain breaks into several fragments, which attach at the rim of the cluster. The highly ordered cluster remains without defects. Figure 10b shows the merging of three clusters and the reordering process under the influence of subsequent field rotations. As seen in Fig. 10c, the inner reorganization dynamics along the inner boundaries may leave isolated vacancies and defects which can be attributed to the steric obstruction of geometric reordering. This already gives a first indication of the concentration dependency on the spatial ordering of two-dimensional particle arrays.

A typical monolayer resulting from the ordering process in a rotating magnetic field is presented in Fig. 11. Large areas of highly ordered particles can be observed. The corresponding Fourier transform obtained from an image analysis of the spatial particle distribution shows a high degree of local hexagonal symmetry (Fig. 11a). Globally, ordered areas are grouped in grain-like superstructures. Along the grain boundaries, isolated vacancies can be found, which are the results of reorganization processes as shown above. Also, a very small degree of below 5 % area coverage of double layers is present (Fig. 11c). The dynamics of the cluster growth depends on the particle concentration and the rotation frequency of the applied field. In Fig. 12, the main findings are summarized. Measurements were carried out with two different concentrations of 0.2 mg/ml (red data points) and 1 mg/ml (blue data points). In addition, to study cluster growth by iterative concentration replenishments, a 1-µl droplet has been subsequently added to evaporated samples. As a reference, we chose similar solution droppings without the presence of an external magnetic field. In that case, only a low number of small agglomerates can be found and microscopy images of these samples reveal no existence of a local symmetry. Particles are randomly dispersed along the substrate and, therefore, a defect concentration cannot be discussed.

The evaporation of the particle suspension under the exposure to a rotating magnetic field induces a local symmetry. As shown in Fig. 12a, the size of the resulting

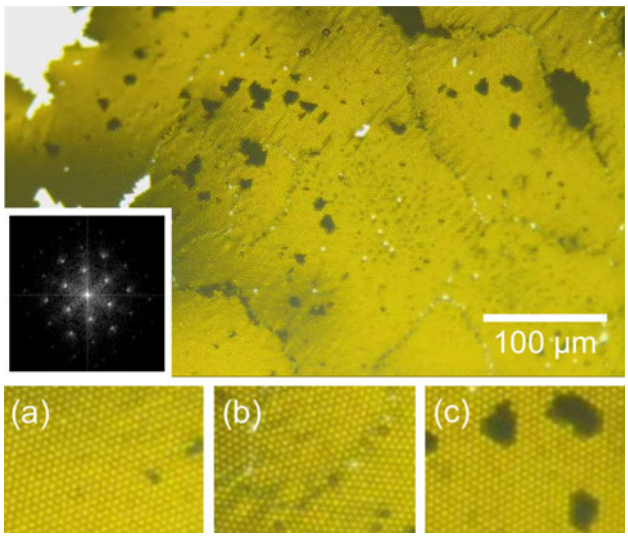

Fig. 11 Monolayer consisting of magnetic beads. The *inset* shows an FFT image of a grain structure which reveals a high degree of hexagonal ordering. Besides grain structures (**a**), grain boundaries (**b**) and second layer growth (**c**) can be identified (reprinted with permission from Weddemann et al. 2010a. Copyright 2010, American Chemical Society)

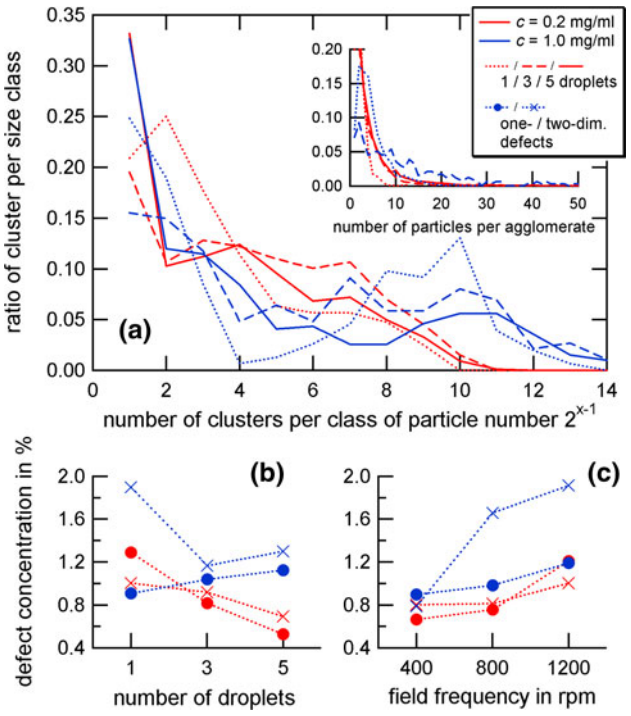

Fig. 12 **a** Cluster growth and defect concentration within the agglomerates for concentrations of 0.2 and 1.0 mg/ml. The *inset* shows the results without the employment of a magnetic field. The defect concentration is dependent on the number of particles on the substrate (**b**) and the rotation frequency of the external field (**c**) (reprinted with permission from Weddemann et al. 2010a. Copyright 2010, American Chemical Society)

agglomerates shifts to increasingly higher numbers if higher particle concentrations are provided.

Two different approaches may be pursued to realize a higher total number of particles: (1) conducting the spotting procedure with a higher initial particle concentration or (2) subsequent spotting of droplets onto the same substrate upon evaporation. The observed growth mechanism can be understood in a similar way to the Ostwald ripening dynamics (Ostwald 1896) in nanoparticle fabrication. Instead of the formation of many small assemblies, the growth of few larger agglomerates is preferred. The size of the agglomerates is not influenced by a variation of the rotation frequency of the external field. The results for the defect concentrations are presented in Fig. 12b, c. For low particle concentrations, the number of defects reduces with an increasing number of particles in the sample (Fig. 12b, red lines). Instead, if highly concentrated suspensions are employed, an increase in the number of defects can be reported. The reason for this behavior can be found in the lower degree of accessible free volume in the case of highly concentrated particle solutions. The resulting inhibition of the geometric reordering processes is comparable to the phenomena presented in Fig. 10c. Therefore, a higher defect concentration is obtained for the employment of higher particle concentrations. Further, the employment of higher rotation frequencies entails a higher defect concentration (Fig. 12c). If the timespan for a full field rotation becomes increasingly shorter, it may drop below the timescale required for reorganization dynamics to complete.

The proposed method is easy to apply since only an external rotating magnetic field is required, which may for example be created by a magnetic stirrer for the support of chemical reactions. The average grain size obtained by the consecutive spotting of three 1-µl droplets is about 463 particles, and the corresponding grain area is $\sim$2,850 µm^2. Similar results were achieved by other approaches, such as the sedimentation strategy proposed by Riley and Lidell (2010). However, the proposed direct employment of dipolar coupling offers a fast reliable way to realize large sheets of locally highly ordered two-dimensional particle arrays within a liquid phase.

5.2 Ordering of nanoscale particles

In all the experiments discussed above, magnetic microbeads took the role as the dipolar component. It is not immediately possible to tell whether a similar approach would be successful on the nanoscale due to different dominating physical contributions. While the microscale is governed by steric repulsion and magnetic interactions (Petousis et al. 2007), van der Waals forces and thermal agitation gain importance on the nanoscale. It is well known that a long range ordering of magnetic nanoparticles can be induced by a stationary, homogeneous magnetic field (Weddemann et al. 2010b). Furthermore, the interplay between ferrofluids and magnetic (Erb et al. 2009), as well as non-magnetic, material may be used to generate regularly ordered structures (Yellen et al. 2005: Krebs et al. 2009). In order to investigate the ordering of magnetic nanoparticles under the influence of a magnetic field that rotates perpendicular to the field direction, a spotting procedure similar to the method discussed in the previous section for microparticles was employed (Regtmeier et al. 2012). Typical resulting assemblies of 6-nm Co nanoparticles are presented in Fig. 13. Two different cobalt concentrations, $c_{\text{low}} = 3.66$ mmol/l and $c_{\text{high}} = 35.95$ mmol/l, of the nanoparticle suspension were chosen.

A quantitative analysis of SEM images similar to those in Fig. 13 is shown in Fig. 14a, b in the case of low and high concentrations, respectively. The particle ratios were obtained via a manual counting evaluation. As seen in Fig. 14a, b, the rotating magnetic field leads to the formation of larger clusters compared to the reference samples, which were prepared without the influence of a magnetic field (dotted lines). For both concentrations employed, the influence of the magnetic field is evident

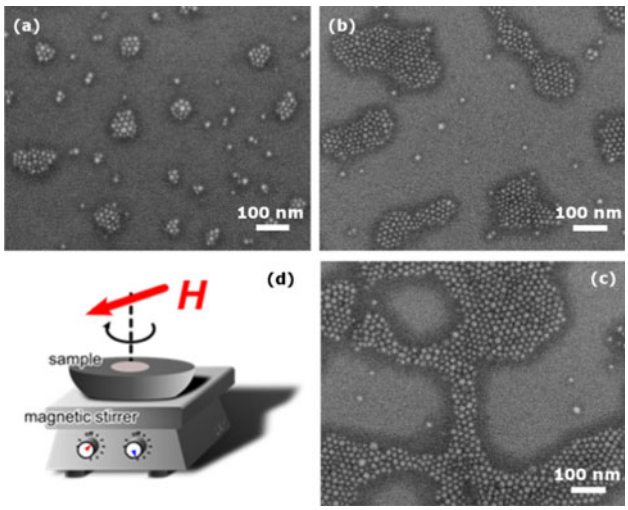

Fig. 13 Scanning electron micrograph of cobalt nanoparticle asemblies which result from cobalt concentrations of (**a**) $c_{low} = 3.66$ mmol/l and (**b**, **c**) $c_{high} = 35.95$ mmol/l. The experimental setup is schematically illustrated in (**d**) (Regtmeier et al. 2012)

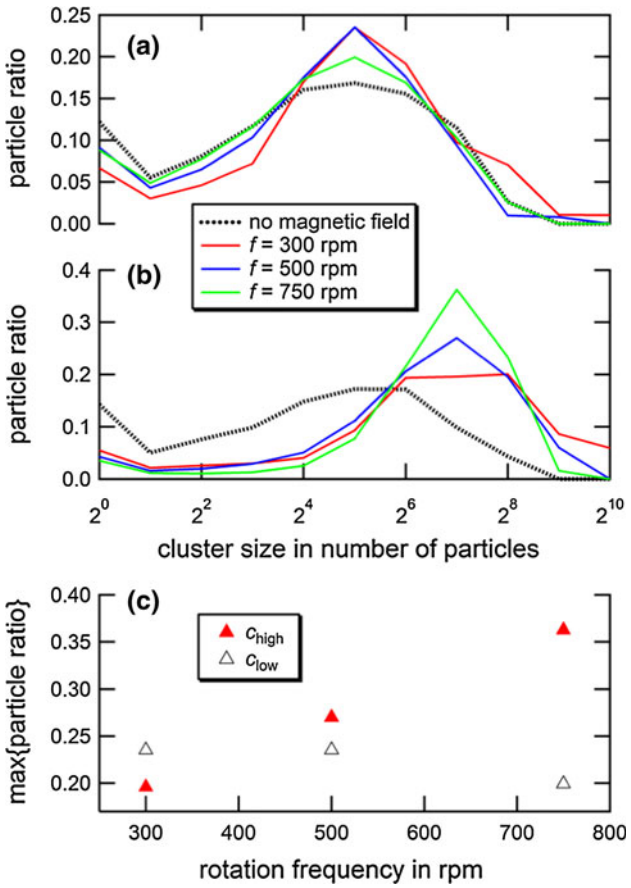

Fig. 14 Particle ratio distributions which result from magnetic field rotation frequencies of 300, 500 and 750 rpm for the respective concentration (**a**) c_{low} and (**b**) c_{high}. (**c**) The frequency dependency of the particle ratio distribution is influenced by the nanoparticle concentration (Regtmeier et al. 2012)

from the data presented, as more efficient cluster growth is obtained and the number of single particles decreases significantly. However, the underlying dynamics may differ, which can be concluded from Fig. 14c, since the dependence of the maximum of the particle ratio distribution on the rotation frequency of the magnetic field changes with the concentration. In the case of a low particle concentration, the maximum of the particle ratio decreases with increasing rotation frequency. Instead, for the high concentration case, an increase in the maximum is found if higher rotation frequencies are applied.

The underlying dynamics, which leads to the formation of nanoparticle assemblies, are governed by the interplay of the magnetic long ranging forces and the van der Waals interaction, which is only relevant at very short distances.

Thermal effects may be omitted in the following discussion, since magnetic coupling is much stronger than thermal contributions if an external magnetic field is applied. The most important contribution, which leads to the different frequency dependence of the nanoparticle cluster growth, is the average distance between neighboring particles, which changes with the concentration. For the low concentration case, a high rotation frequency of the external magnetic field may lead to oscillations of the nanoparticles close to their initial position, similar to the case of the reference samples, where the oscillations are dominated by thermal contributions. Therefore, the timescales for particles to interact with contiguous particles are very short, giving rise to a similar particle ratio distribution as obtained in the reference case. By reduction of the rotation frequencies, the relevant timescales are enlarged, which eases the formation of clusters. Consequently, the maximum of the particle ratio distribution shown in Fig. 14a becomes slightly more developed and, especially, the standard deviation of the distribution is decreased by reduction of the rotation frequency. In the case of high particle concentrations, the average inter-particle distances are reduced, which results in strongly increased timescales for the particle–particle interaction. Agglomeration processes due to attractive magnetic forces occur on relatively short timescales, which lead to the formation of clusters of high particle numbers (Fig. 14b) and reduce the amount of individual particles. In this case of long interaction timescales, the increase of the rotation frequency leads to an increase in the mobility of particles during the agglomeration, which allows for the formation of larger clusters as presented in Fig. 14c.

6 Conclusions and outlook

We have shown that microfluidic components can strongly benefit from the employment of dipolar interaction of

magnetic particles. To understand the formation dynamics and stability criteria, fundamental investigations were presented. Applications of both static and rotating magnetic field, which employ micron-sized magnetic particles as active components, combine the advances in established magneto-based MEMS and NEMS devices with progresses in the research of on-demand configurable matter. Various functional tasks such as particle guidance, pumping, positioning of agglomerates and surface patterning can be achieved. In addition to the further investigation and development of microfluidic systems based on the employment of magnetic microparticles, especially the approaches which extend the processes to smaller particle sizes are promising and will be part of future work.

Acknowledgments The author would like to thank the FOR 945 for financial support in the framework of the project 3. Alexander Weddemann gratefully acknowledges funding from the Alexander von Humboldt foundation.

References

Bossis G, Lacis S, Meunier A, Volkova O (2002) Magnetorheological fluids. J Magn Magn Mat 252:224–228

Brigadnov IA, Dorfmann A (2005) Mathematical modeling of magnetorheological fluids. Continuum Mech Thermodyn 17:29–42

Deng T, Whitesides GM, Radhakrishnan M, Zabow G, Prentiss M (2001) Manipulation of magnetic microbeads in suspension using micromagnetic systems fabricated with soft lithography. Appl Phys Lett 78(12):1775–1777

Derks RJS, Frijns AJH, Prins MWJ, Dietzel A (2010) Multibody interactions of actuated magnetic particles used as fluid drivers in microchannels. Microfluid Nanofluid 9:357–364

Erb RM, Son HS, Samanta B, Rotello VM, Yellen BB (2009) Magnetic assembly of colloidal superstructures with multipole symmetry. Nature 457:999–1002

Fonnum G, Johansson C, Molteberg A, Mørup S, Aksnes E (2005) Characterisation of Dynabeads® by magnetization measurements and Mössbauer spectroscopy. J Magn Magn Mater 293:41–47

Furst EM, Gast AP (1999) Micromechanics of dipolar chains using optical tweezers. Phys Rev Lett 82:4130–4133

Gast AP, Zukoski CF (1989) Electrorheological fluids as colloidal suspensions. Adv Colloid Interface Sci 30:153–202

Gijs MAM (2004) Magnetic bead handling on-chip: new opportunities for analytical applications. Microfluid Nanofluid 1:22–40

Ginder JM, Davis LC (1994) Shear stresses in magnetorheological fluids: role of magnetic saturation. Appl Phys Lett 65:3410–3412

Ginder JM, Davis LC, Elie LD (1996) Rheology of magnetorheological fluids: models and measurements. Int J Modern Phys B 10:3293–3303

Haukanes B-I, Kvam C (1993) Application of magnetic beads in bioasays. Nat Biotechnol 11:60–63

Jackson JD (1975) Classical electrodynamics, 2nd edn. Wiley, New York

Kalontarov M, Tolley MT, Lipson H, Erickson D (2009) Hydrodynamically driven docking of blocks for 3D fluidic assembly. Microfluid Nanofluid 9:551–558

Karle M, Wöhrle J, Miwa J, Paust N, Roth G, Zengerle R, von Stetten F (2011) Controlled counter-flow motion of magnetic bead chains rolling along microchannels. Microfluid Nanofluid 10:935–939

Kim YS, Park IH (2010) FE analysis of magnetic particle dynamics on fixed mesh with level set function. IEEE Trans Magn 46(8):3225–3228

Kose AR, Fischer B, Mao L, Koser H (2009) Label-free cellular manipulation and sorting via biocompatible ferrofluids. Proc Natl Acad Sci 106:21478–21483

Krebs MD, Randall ME, Yellen BB, Samanta B, Bajaj A, Rotello VM, Alsberg E (2009) Formation of ordered cellular structures in suspension via label-free negative magnetophoresis. Nano Lett 9:1812–1817

Lacharme F, Vandevyver C, Gijs MAM (2009) Magnetic beads retention device for sandwich immunoassay: comparison of off-chip and on-chip antibody incubation. Microfluid Nanofluid 7:479–487

LaMer VK, Dinegar RH (1950) Theory, production and mechanism of formation of monodispersed hydrosols. J Am Chem Soc 72:4847–4854

Laroze D, Vargas P, Cortes C, Gutierrez G (2008) Dynamic of two interacting dipoles. J Magn Magn Mater 320:1440–1448

Love LJ, Jansen JF, McKnight TE, Roh Y, Phelps TJ, Yeary LW, Cunningham GT (2005) Ferrofluid field induced flow for microfluidic applications. IEEE Transact Mechatron 10:68–76

Mao L, Elborai S, He X, Zahn M, Koser H (2011) Direct observation of closed-loop ferrohydrodynamic pumping under traveling magnetic fields. Phys Rev B 84:104431

Melle S, Calderón OG, Rubio MA, Fuller GG (2003) Microstructure evolution in magnetorheological suspensions governed by Mason number. Phys Rev E 68:041503

Mørup S, Hansen MF, Frandsen C (2010) Magnetic interactions between nanoparticles. Beilstein J Nanotechnol 1:182–190

Moskowitz R, Rosensweig RE (1967) Nonmechanical torque-driven flow of a ferromagnetic fluid by an electromagnetic field. Appl Phys Lett 11:301–303

Niarchos D (2003) Magnetic MEMS: key issues and some applications. Sensors Actuators A: Phys 109:166–173

Østergaard S, Blankenstein G, Dirac H, Leistiko O (1999) A novel approach to the automation of clinical chemistry by controlled manipulation of magnetic particles. J Magn Magn Mater 194:156–162

Ostwald W (1896) Lehrbuch der allgemeinen Chemie: part I, vol 2. Veit, Leipzig

Pamme N (2006) Magnetism and microfluidics. Lab Chip 6:24–38

Pamme N, Manz A (2003) On-chip free flow magnetophoresis: continous flow separation of magnetic particles and agglomerates. Lab Chip 3:187–192

Petousis I, Homburg E, Derks R, Dietzel A (2007) Transient behavior of magnetic micro-bead chains rotating in a fluid by external fields. Lab Chip 7:1746–1751

Radoszkowicz L, Presiado I, Erez Y, Nachliel E, Huppert D, Gutman M (2011) Time-resolved emission of flavin adenine dinucleotide in water and water–methanol mixtures. Phys Chem Chem Phys 13:12058–12066

Regtmeier A, Wittbracht F, Rempel T, Mill N, Peter M, Weddemann A, Mattay J, Hütten A (2012) Uniform growth of clusters of magnetic nanoparticles in a rotating magnetic field. J Nanopart Res (submitted)

Riley EK, Lidell CM (2010) Confinement-cotrolled self assembly of colloids with simultaneous isotropic and anisotropic cross-section. Langmuir 26:11648–11656

Rosensweig RE (1996) "Negative viscosity" in a magnetic fluid. Science 271:614–615

Sawetzki T, Rahmouni S, Bechinger C, Marr DWM (2008) In situ assembly of linked geometrically coupled microdevices. Proc Natl Acad Sci USA 105:20141

Shliomis MI, Morozov KI (1994) Negative viscosity of ferrofluid under alternating magnetic field. Phys Fluids 6(8):2855–2861

Sugimoto T (2001) Monodispersed particles. Elsevier, Amsterdam

Tang X, Conrad H (2000) An analytical model for magnetorheological fluids. J Phys D Appl Phys 33:3026–3032

Vuppu A, Garcia AA, Hayes MA (2003) Video microscopy of dynamically aggregated paramagnetic particle chains in an applied rotating magnetic field. Langmuir 19:8646–8653

Weddemann A, Wittbracht F, Auge A, Hütten A (2009) A hydrodynamic switch: microfluidic separation system for magnetic beads. Appl Phys Lett 94:173501

Weddemann A, Wittbracht F, Eickenberg B, Hütten A (2010a) Magnetic field induced assembly of highly ordered two-dimensional particle arrays. Langmuir 26:19225–19229

Weddemann A, Ennen I, Regtmeier A, Albon C, Wolff A, Eckstädt K, Mill N, Peter MKH, Mattay J, Plattner C, Sewald N, Hütten A (2010b) Review and outlook: from single nanoparticles to self-assembled monolayers and granular GMR sensors. Beilstein J Nanotechnol 1:75–93

Weddemann A, Wittbracht F, Auge A, Hütten A (2011) Particle flow control by induced dipolar interaction of superparamagnetic microbeads. Microfluid Nanofluid 10:459–463

Wittbracht F, Eickenberg B, Weddemann A, Hütten A (2011) Towards a programmable microfluidic valve: Formation dynamics of two-dimensional magnetic bead arrays in transient magnetic fields. J Appl Phys 109:114503

Wittbracht F, Weddemann A, Eickenberg B, Zahn M, Hütten A (2012) Enhanced fluid mixing and separation of magnetic bead agglomerates based on dipolar interaction in rotating magnetic fields. Appl Phys Lett 100:123507

Yeh CS, Chen KC (1997) A thermodynamic model for magnetorheological fluids. Continuum Mech Thermodyn 9:273–291

Yellen BB, Hovorka O, Friedman G (2005) Arranging matter by magnetic nanoparticle assemblers. Proc Natl Acad Sci 102:8860

Zahn M, Pioch LL (1999) Ferrofluid flows in AC and travelling wave magnetic fields with effective positive, zero or negative dynamic viscosity. J Magn Magn Mater 201:144–148

Zborowski M, Liping S, Moore LR, Williams S, Chalmers JJ (1999) Continuous cell separation using novel magnetic quadrupole flow sorter. J Magn Magn Mater 194:224–230

Zhu T, Marrero F, Mao L (2010) Continuous separation of non-magnetic particles inside ferrofluids. Microfluid Nanofluid 9:1003–1009

Zhu T, Lichlyter DJ, Haidekker MA, Mao L (2011a) Analytical model of microfluidic transport of non-magnetic particles in ferrofluids under the influence of a permanent magnet. Microfluid Nanofluid 10:1233–1245

Zhu T, Cheng R, Mao L (2011b) Focusing microparticles in a microfluidic channel with ferrofluids. Microfluid Nanofluid 11:695–701